

Follow Everything: A Leader-Following and Obstacle Avoidance Framework with Goal-Aware Adaptation

Qianyi Zhang¹, Shijian Ma², Boyi Liu³, Jingtai Liu^{†,1}, Jianhao Jiao^{†,4} and Dimitrios Kanoulas⁴

Abstract—Robust and flexible leader-following is a critical capability for robots to integrate into human society. While existing methods struggle to generalize to leaders of arbitrary form and often fail when the leader temporarily leaves the robot’s field of view, this work introduces a unified framework addressing both challenges. First, traditional detection models are replaced with a segmentation model, allowing the leader to be anything. To enhance recognition robustness, a distance frame buffer is implemented that stores leader embeddings at multiple distances, accounting for the unique characteristics of leader-following tasks. Second, a goal-aware adaptation mechanism is designed to govern robot planning states based on the leader’s visibility and motion, complemented by a graph-based planner that generates candidate trajectories for each state, ensuring efficient following with obstacle avoidance. Simulations and real-world experiments with a legged robot follower and various leaders (human, ground robot, UAV, legged robot, stop sign) in both indoor and outdoor environments show competitive improvements in follow success rate, reduced visual loss duration, lower collision rate, and decreased leader-follower distance. Visit the [website](#) for the video and code.

I. INTRODUCTION

Recent advances in visual perception, robot navigation, and large models have enabled robots to follow leaders with increased safety and intelligence [1]–[3]. Serving as powerful assistants, robots can follow explorers to carry more supplies, guide customers and introduce products in shopping malls, help police track and capture suspects, and more [4]–[6].

While existing research on leader-following typically focuses on following a specific pedestrian detected using lightweight camera-based [7], LiDAR-based [8], or multimodal-based [9], [10] approaches, often assisted by Kalman filters [11], we argue that a robot’s following capability should extend beyond this limited scope, enabling it to follow leaders of any shape or type, including humans, animals, vehicles, irregular objects, and even other robots. To support this, instead of relying on conventional detection models designed for specific categories, this work adopts a segmentation model, SAM2 [12], which enables flexible selection of leader masks with arbitrary shapes. This shift in logic enables anything to be a leader, regardless of its shape or type. Unlike the work [13], which only uses SAM2 with RGB image input, our method better accommodates the

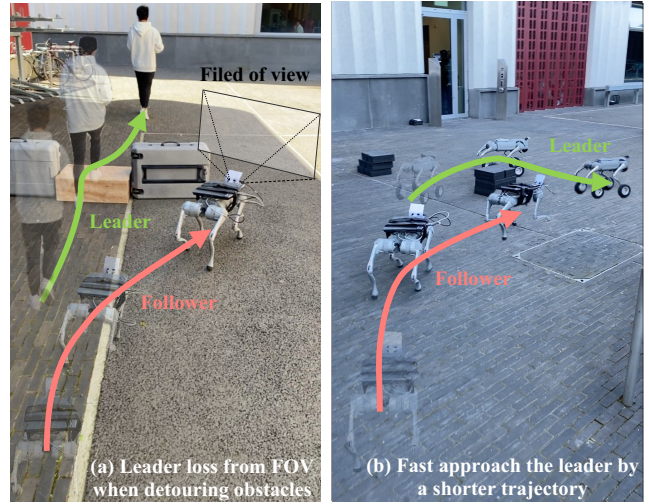


Fig. 1. Illustration of the challenges in leader-following tasks. (a) When the leader steps over a box that the follower must detour around, the leader leaves the follower’s field of view. (b) The follower is expected to follow the leader via a shorter trajectory, not by replicating the leader’s past path.

leader-following task, where the depth image is accessible and the distance between the leader and the robot fluctuates within a certain range. A distance frame buffer is introduced (see Sec. II) on top of the existing model [12], enhancing tracking robustness, particularly when the leader re-enters the robot’s field of view (FOV) after a temporary loss.

However, both detection- and segmentation-based methods are inherently limited by the FOV constraints of onboard sensors [14]. As a result, once the leader moves beyond the sensor’s FOV, the robot may fail to detect the leader, leading to awkward hesitation or inaction [15]. To address this limitation, some studies [16] have incorporated sonar sensors to detect the leader’s footsteps; however, this approach tends to perform poorly in crowded environments. Other methods rely on the leader carrying lightweight beacons, such as infrared antennas [17] or wave emitters [18], [19], but requiring the leader to bear additional equipment is often impractical.

While these methods do help alleviate the issue of losing the leader by improving the perception robustness, some instances are inevitable [20]. For example, when a mobile robot follows a human walking out of a room, the human will naturally disappear from the robot’s current FOV after exiting. Similarly, when a ground robot follows a UAV, the UAV may fly over obstacles that the ground robot must detour around, making it easy to lose visual contact during the process [13]. Therefore, we argue that it is impractical

¹ Institute of Robotics and Automatic Information System, Nankai University, Tianjin 300350, China. ² Electrical and Computer Engineering Department, Hong Kong University of Science and Technology, China. ³ Centre for Data Science, University of Macau, China. ⁴ Department of Computer Science, University College London, UK.

[[†]] The corresponding authors. Email: jianhao.jiao@ucl.ac.uk. This work is supported by the National Natural Science Foundation of China under Grant 62173189 and UK Research and Innovation Future Leaders Fellowship (RoboHike, Grant No. MR/V025333/1).

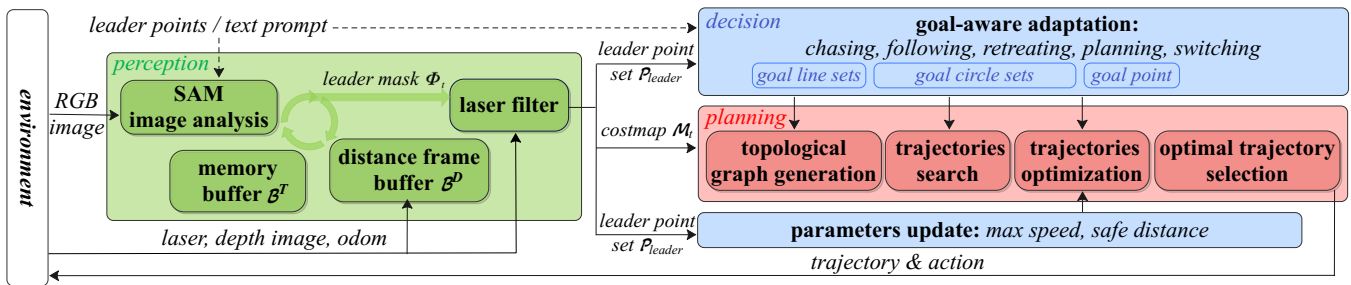


Fig. 2. Illustration of the proposed leader-following and obstacle avoidance framework. Given a leader prompt and an RGB image, SAM segments the leader mask with the aid of both a memory buffer and a distance frame buffer. The segmented leader is then filtered from raw laser point clouds to produce a leader point set, which is passed to the goal-aware adaptation module to determine the current goal state and relevant parameters. Meanwhile, a costmap is generated and sent to the planning module, which computes the optimal trajectory based on the selected goal state and parameters.

to rely solely on the perception module to handle such cases. The planning module should work in conjunction with perception and be capable of actively re-locating the leader after temporary loss, thereby enhancing the robustness of the following behavior—for instance, by adaptively adjusting the robot’s speed when the leader moves quickly or becomes distant, and maintaining an appropriate safety distance to reduce the risk of losing the leader. In addition, when the leader approaches the robot, the robot should be able to retreat accordingly to avoid getting too close. This helps prevent both failure in capturing the leader’s mask due to excessive proximity and the collision risk when the leader steps backward without being aware of the robot’s position.

While most existing approaches overlook the issues mentioned above, simply treating the leader’s last known position as a waypoint and planning motions using PID-based controllers [13], MPC-based controllers [21], sampling-based trajectories [22], optimization-based trajectories [23], or learning-based approaches [24], the goal-aware adaptation proposed in this work systematically considers these factors within an integrated framework (see Sec.III).

Five states are defined within the goal-aware adaptation framework to address various leader-robot interaction scenarios: (a) The *following* state is activated when the leader is within the robot’s field of view, and the robot’s goal is a set of points on a variable-radius circle centered on the leader. The environment is modeled as a topological graph to generate and optimize candidate trajectories, whose endpoints can slide along the circular goal set. The robot’s maximum speed is determined by its relative state to the leader, while the safety distance (circle radius) is dynamically adjusted based on the leader’s motion uncertainty. (b) The *chasing* is activated when the leader is visible but at a considerable distance, and the robot’s goal is a set of lines pointing toward the leader. The robot then moves at its maximum allowable speed to minimize the risk of losing the leader. (c) The *retreating* state is activated when the leader moves toward the robot. The goal remains on the circular point set, but additional constraints ensure that the robot maintains its orientation toward the leader while retreating to a safe distance. (d) The *planning* state is triggered when the leader leaves the robot’s FOV. The robot uses the leader’s last known state as

a temporary goal and computes a retracing trajectory via the topological graph. (e) The *switching* state allows dynamic leader replacement. External prompts, interpreted by a large language model [12], generate a new leader mask, enabling the robot to follow a newly assigned leader.

In summary, this work presents a unified framework for robustly leader-following and obstacle avoidance. The main contributions are as follows:

- A segmentation module with a distance frame buffer is introduced to enable anything to be a leader.
- A goal-aware adaptation strategy is proposed to enable state switching for robust leader-following.
- A graph-based trajectory planner is developed to produce candidate trajectories for safe following.

II. LEADER SEGMENTATION WITH DISTANCE FRAME BUFFER

Given the initial RGB image I_0 and a set of leader point prompts (often manually selected on the image; see Fig.3a), the segmentation model, EVF-SAM [12], automatically expands the prompts to segment the full leader, producing an embedding η_0 and its corresponding mask ϕ_0 . At each subsequent timestep t , the top n historical leader embeddings with the highest confidence scores are updated and maintained in a temporal memory buffer:

$$\mathcal{B}^T = \{\eta_i, \eta_j, \eta_k, \dots\}_n \quad (1)$$

These embeddings, along with the current image I_t , are utilized to generate the current leader embedding and mask:

$$\eta_t, \phi_t = \text{SAM}(I_t, \mathcal{B}^T) \quad (2)$$

This temporal memory buffer performs well when the leader remains continuously within the robot’s FOV. However, as illustrated in Fig.1(a), the leader may be temporarily lost when the robot detours around obstacles. Just before this loss, the leader often appears at the edge of the robot’s FOV, resulting in partial and low-quality embeddings. Despite their poor quality, these embeddings may still dominate the memory buffer due to their relatively higher confidence scores, since embeddings that capture the leader’s full body shape differ significantly from the current appearance of the leader in the image [13]. This may mislead the robot to

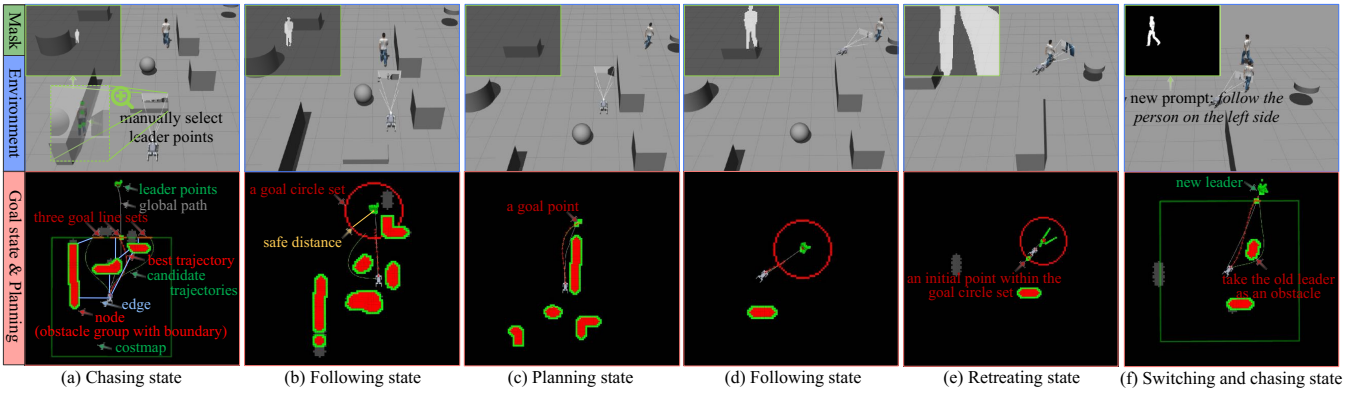


Fig. 3. Illustration of goal-aware adaptation and graph-based planning in a demonstration. (a) SAM segments the leader after manually selecting a few leader points. *Chasing* is activated as the leader is far away. (b) *Following* is triggered when the robot gets closer, maintaining a safe distance. (c) *Planning* is activated when the leader exits the robot’s FOV, guiding the robot to the last known leader pose. (d) *Following* resumes once the leader is visible again. (e) *Retreating* is triggered when the leader steps back. (f) A new prompt activates *Switching*, followed by *Chasing* as the new leader is distant.

bootstrap toward incorrect directions. As a result, when the leader reappears later, the robot may fail to retrace the leader accurately, even if the complete leader is in front of it.

To address this issue, the distance frame buffer \mathcal{B}^D is introduced. Unlike the temporal memory buffer, which operates along the time dimension, the distance frame buffer leverages spatial information enabled by depth image input. In leader-following tasks, the distance d_i between the robot and the leader varies dynamically due to speed differences or detours. For each relative distance segment (with a margin Δd), the leader embedding with the highest confidence score is stored and updated in the distance frame buffer:

$$\begin{aligned} \mathcal{B}^D &= \{\eta_i, \eta_j, \eta_k, \dots\}_n \\ \eta_t, \phi_t &= \text{SAM}(I_{t_i}, \mathcal{B}^T, \mathcal{B}^D) \end{aligned} \quad (3)$$

By incorporating both temporal and spatial memory, this mechanism significantly improves SAM’s ability to retrace and re-identify the leader after temporary visual loss.

Aligning the leader mask ϕ_t with the corresponding depth image, the leader can be extracted as a point set $\mathcal{P}_{leader} = \{\mathbf{p}_1, \mathbf{p}_2, \dots, \mathbf{p}_m\}$, where each point $\mathbf{p}_i = (x, y, z)$. These points are then used to filter the point cloud transformed from the laser scan, and the remaining points form a costmap \mathcal{M}_t .

III. GOAL-AWARE ADAPTATION AND GRAPH-BASED TRAJECTORY PLANNING

A. Parameters Adaptation

During planning, two key parameters related to the leader’s state influence the robot’s behavior: the maximum speed V_t^{\max} and the safe distance D_t .

The robot’s maximum speed is determined by the relative distance between the robot and the leader, as well as the leader’s estimated velocity. The leader’s position \bar{p}_l is obtained by averaging the segmented leader point set \mathcal{P}_{leader} , and the leader’s velocity \bar{v}_l is estimated based on the positional difference over a fixed time interval. The maximum robot speed during the current planning is then computed as:

$$V_t^{\max} = \text{Clip}(\alpha_1 |\bar{v}_l| + \alpha_2 |\bar{p}_l - p_r|, 0, V_{max}) \quad (4)$$

where α_1 and α_2 are predefined scaling factors, p_r is the robot’s position, $|\cdot|$ denotes the vector norm, and V^{\max} is the maximum velocity the robot can physically execute. The $\text{Clip}(\cdot)$ function ensures the computed value respects the robot’s dynamic constraints.

To ensure safe interaction, the robot maintains a larger safe distance D_t when the leader’s motion is more uncertain. A Kalman filter is used to estimate the leader’s state, where the Normalized Innovation Squared (NIS) [11] value serves as an indicator of prediction uncertainty. Based on this, the safe distance is dynamically adjusted as:

$$D_t = \text{Clip}(\alpha \text{NIS}, D^{\min}, D^{\max}) \quad (5)$$

where D^{\min} and D^{\max} are predefined lower and upper bounds, and α is a scaling factor.

B. Goal States Adaptation and Trajectory Planning

The transition between states is governed by conditions including whether the leader is within the robot’s FOV, whether it lies within the costmap, the distance between the robot and the leader, and whether a new leader is assigned.

The *chasing* state (see Fig.3a) is activated when the leader is within the robot’s FOV but outside the current costmap range. In this state, the robot’s primary task is to navigate around nearby obstacles and chase the leader as quickly as possible. Following prior work [25], [26], adjacent obstacle points in the costmap are clustered into obstacle groups, each outlined by a boundary. Each obstacle group with its boundary forms a node \mathcal{N}_i in the topological graph. For any two boundaries with indices i and j , their shortest collision-free connection is defined as an edge $\mathcal{E}_{i,j}$.

Unlike conventional approaches that select the local goal as the intersection point between the global path and the costmap boundary, the chasing state extends this local path along the costmap edge to form a goal line of length L_t , which is proportional to the distance between the robot p_r and the leader \bar{p}_l :

$$L_t = \alpha(|p_r - \bar{p}_l| - \frac{W_{map}}{2}) \quad (6)$$

where W_{map} is the costmap width and α is a scaling factor.

The whole goal line is separated at the locations where it intersects with obstacles, resulting in several sub-goal line sets \mathcal{G}_i , which are then added as additional nodes to the topological graph along with their corresponding connections.

Several generalized trajectories can be generated over the topological graph using depth-first search, with each one \mathcal{T} following the form:

$$\mathcal{T} = p_r \rightarrow \mathcal{E}_{r,i} \rightarrow \widehat{\mathcal{N}}_i \rightarrow \mathcal{E}_{i,j} \rightarrow \widehat{\mathcal{N}}_j \rightarrow \dots \rightarrow \mathcal{G}_k \quad (7)$$

Since each obstacle node \mathcal{N}_i can be detoured in either a clockwise or counter-clockwise direction, a generalized trajectory \mathcal{T} containing n nodes can yield up to 2^n distinct trajectory candidates τ . To eliminate semantically redundant trajectories that represent the same detour behavior, we apply the concept of trajectory homotopy classes [27], [28] to prune equivalent candidates. The remaining trajectories are then optimized in parallel.

Following the time-optimal optimization framework [29], in addition to standard kinematic, dynamic (with the max speed V^{max}), and obstacle-avoidance constraints, an additional goal constraint is introduced here:

$$\begin{aligned} & \left| \overrightarrow{\mathcal{G}_k^{start} \mathcal{G}_k^{end}} \times \overrightarrow{\mathcal{G}_k^{start} p_\tau^{end}} \right| = 0 \\ 0 & \leq \overrightarrow{\mathcal{G}_k^{start} \mathcal{G}_k^{end}} \cdot \overrightarrow{\mathcal{G}_k^{start} p_\tau^{end}} \leq \left| \overrightarrow{\mathcal{G}_k^{start} p_\tau^{end}} \right| \end{aligned} \quad (8)$$

where \mathcal{G}_k^{start} and \mathcal{G}_k^{end} denote the endpoints of a goal set \mathcal{G}_k . The trajectory end point p_τ^{end} is allowed to slide along \mathcal{G}_k , enhancing smoothness and time optimality. Among all the trajectories, the one with the least time to its goal is selected as the best trajectory and executed by the robot.

The *following* state (see Fig.3b and Fig.3d) follows a principle similar to that of the *chasing* state. The main difference is that the leader is now within the robot's costmap. Instead of goal line sets in the *chasing* state, the candidate goal points are sampled on a circle centered at the leader, with a radius equal to the safe distance D_t . Similarly, these points are segmented by obstacles into several sub-goal circle sets \mathcal{G}_i .

During the optimization, the end point p_τ^{end} is constrained within the goal circle set \mathcal{G}_k , and its orientation θ_τ^{end} is constrained to head to the leader to reduce the risk of loss:

$$\begin{aligned} \overrightarrow{\bar{p}_l \mathcal{G}_k^{start}} \times \overrightarrow{\bar{p}_l p_\tau^{end}} & \geq 0, & \overrightarrow{\bar{p}_l p_\tau^{end}} \times \overrightarrow{\bar{p}_l \mathcal{G}_k^{end}} & \geq 0 \\ \left| \overrightarrow{\bar{p}_l p_\tau^{end}} \right| & = D_t, & \left| \theta_\tau^{end} - \text{atan}(\bar{p}_l - p_\tau^{end}) \right| & \leq \epsilon \end{aligned} \quad (9)$$

where ϵ is a small threshold.

The *planning* state (see Fig.3c) is activated when the leader is no longer within the robot's field of view. This typically occurs when the robot is detouring around an obstacle, or alternates with the *following* state when the leader is partially occluded. During the optimization, the endpoint of the trajectory p_τ^{end} is constrained to coincide with the last known position \bar{p}_l and orientation $\bar{\theta}_l$ of the leader:

$$\left| p_\tau^{end} - \bar{p}_{leader} \right| \leq \epsilon, \quad \left| \theta_\tau^{end} - \bar{\theta}_{leader} \right| \leq \epsilon \quad (10)$$

The *retreating* state (see Fig.3e) is activated when the leader actively approaches the robot, in which case the robot

is expected to move backward to avoid potential collisions with the leader. The goal circle sets in this state are identical to those used in the *following* state. Among all points within the goal sets, the one closest to the robot is selected as the initial goal, and the endpoint of the trajectory is allowed to slide along the corresponding goal set \mathcal{G}_k . This sliding mechanism follows the same formulation as defined in Equ.9.

The *switching* state (see Fig.3f) is activated when a new leader is assigned, most commonly triggered by a large language model [12]. In this state, both the memory buffer and the distance frame buffer are reset based on the current input. The system then directly transitions to the appropriate subsequent state according to the relative relationship between the robot and the newly assigned leader.

IV. SIMULATION

The simulation evaluates the performance of the proposed leader-following and obstacle avoidance framework, Follow Everything, in a Gazebo simulation environment. The follower robot model is a legged robot, Unitree Go2, with a maximum speed of $V^{max} = 1.5$ m/s and dimensions of 70x31x40 cm. The Realsense D435i is used for leader segmentation, and the Mid360 is employed to generate the point cloud. Four different leader scenarios are tested: a mobile robot as the leader in a playground environment, a UAV as the leader in a forest scenario, a pedestrian as the leader in a factory setting, and a stop sign as the leader in a dynamic scenario. In each test scenario, 10 leader trajectories are recorded using ROSbag and replayed to ensure a fair comparison. Each trajectory is tested four times to minimize the effects of environmental noise, resulting in 40 tests per scenario and 160 tests in total.

Four metrics [23] are considered: (1) the *follow success rate* (defined as successful when the robot maintains a safe distance from the leader and the leader remains in the robot's FOV after the leader reaches its target), which is the most direct measure of the robot's following robustness; (2) the *average leader loss time ratio* (the ratio of time during which the leader is lost from the robot's view to the total test time), which reflects the causes of following failure in detail; (3) the *collision rate* (the ratio of collision occurrences to total 160 tests), which measures the following safety; and (4) the *average distance* (the average distance between the robot and the leader during the total 160 tests), where a larger distance can increase the risk of losing the leader.

Our method, Follow Everything, is compared against four baselines: (1) Alaa [13], which segments the leader using SAM2 and plans trajectories with a PID controller; (2) SA-MPC [21], which detects the leader using YOLO11 and utilizes an enhanced MPC-based planner; (3) FE-N-DFB, an ablated version of our framework that does not incorporate the distance frame buffer; and (4) FE-N-GP, another ablated version of our framework that replaces the graph-based planner with the MPC controller of SA-MPC.

Further details regarding the simulation setup and parameters are available in the [source code](#)¹.

¹<https://follow-everything.github.io>

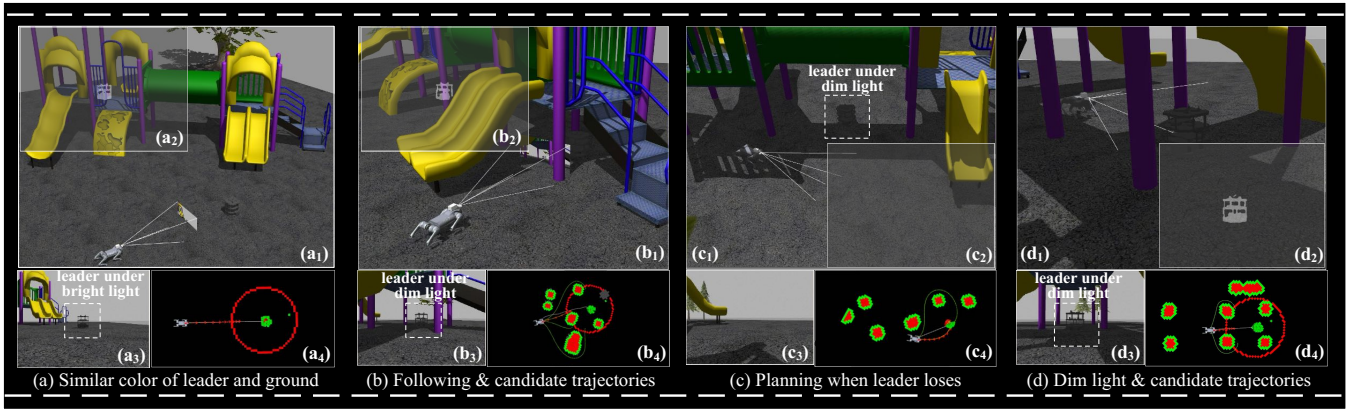


Fig. 4. Simulation for following a mobile robot in a playground. (a) The leader can be robustly segmented even when its color closely resembles the ground. (b) Multiple candidate trajectories are generated for the robot to choose from. (c) When the leader is lost, the planning state enables the follower to actively search for the leader instead of awkwardly stopping in place. (d) Even under dim lighting conditions, the leader can still be robustly segmented.

Mobile robot leader in playground. In this scenario, the leader is a mobile robot whose color closely resembles that of the ground, as shown in Fig.4(a). A building is placed at the center of the scenario, where narrow gaps are just wide enough for both the leader and the follower to pass through.

This scenario presents three major challenges. The first challenge is whether the follower can robustly segment and track the leader under varying lighting conditions. As shown in Fig.4(a), when the leader is outside the slide, the lighting is relatively bright. In contrast, inside the slide (Fig.4b–d), the lighting becomes dim, which can significantly alter the visual features of the leader. This discrepancy often leads to detection or segmentation failures, even when the leader is directly in front of the follower. Such failures are particularly evident in methods that rely on YOLO11 for leader detection. In contrast, the SAM-based memory buffer in Follow Everything continuously updates the leader embedding over time, adapting to illumination changes and reducing the risk of tracking loss. This advantage is reflected in Table.I, where our method greatly outperforms SA-MPC regarding the average leader loss time ratio (10.7% vs 55.3%).

The second challenge is whether the robot can safely follow the leader. As shown in Fig.4(b) and (d), the slide and pillars create several impassable regions. The robot is therefore unable to move directly toward the leader and must instead follow while simultaneously avoiding obstacles. Our graph-based planner addresses this by generating multiple candidate trajectories with distinctive meanings, from which the safest and fastest path can be selected.

The third challenge involves re-identifying the leader after it disappears from the robot’s FOV. As illustrated in Fig.4(c), Our Follow Everything enables the robot to rapidly approach the leader’s last known pose at maximum speed, thereby minimizing the duration of disconnection and achieving the highest follow success rate of 96.9%. In comparison, the ablated variant FE-N-GP does not employ a graph-based planner, nor does it consider the leader’s final orientation or use a speed-maximizing strategy. As a result, its follow success rate drops to 81.3%. When it reaches the leader’s

last known pose, the leader has moved far away, causing the leader to be forever lost. In methods such as Alaa and FE-N-DFB, which rely solely on the temporal memory buffer, as the leader often becomes partially visible in the final frames prior to disappearance, these incomplete embeddings may mislead the model and prevent accurate matching with the current scene, resulting in re-identification success rates of only 21.8% and 62.5%, respectively. In contrast, Follow Everything leverages the distance frame buffer to mitigate this issue, enabling robust leader re-identification.

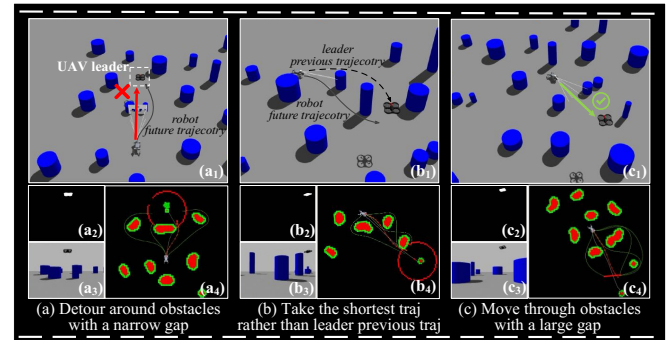


Fig. 5. Simulation for following a UAV in a forest. (a) After the UAV flies through a narrow gap, the robot detours for safety. (b) Rather than replicating the UAV’s historical trajectory, the robot identifies a shorter one. (c) When the gap is wide enough, the robot passes through it for efficiency.

UAV leader in forest. In this scenario, multiple randomly generated cylindrical obstacles are placed to simulate trees in a forest, and the leader is a small UAV. The main challenge lies in balancing following the leader and avoiding obstacles.

When the UAV flies directly over two closely spaced obstacles, as shown in Fig.5(a), the gap between them is too narrow for the follower to pass through. So our Follow Everything enables the robot to promptly detour around the obstacles. During this process, the UAV may temporarily disappear from the robot’s FOV. While the goal-state adaptation transitions from the following state to the planning state, the graph-based planner ensures behavioral consistency by switching the robot’s goal from a circle set to a point.

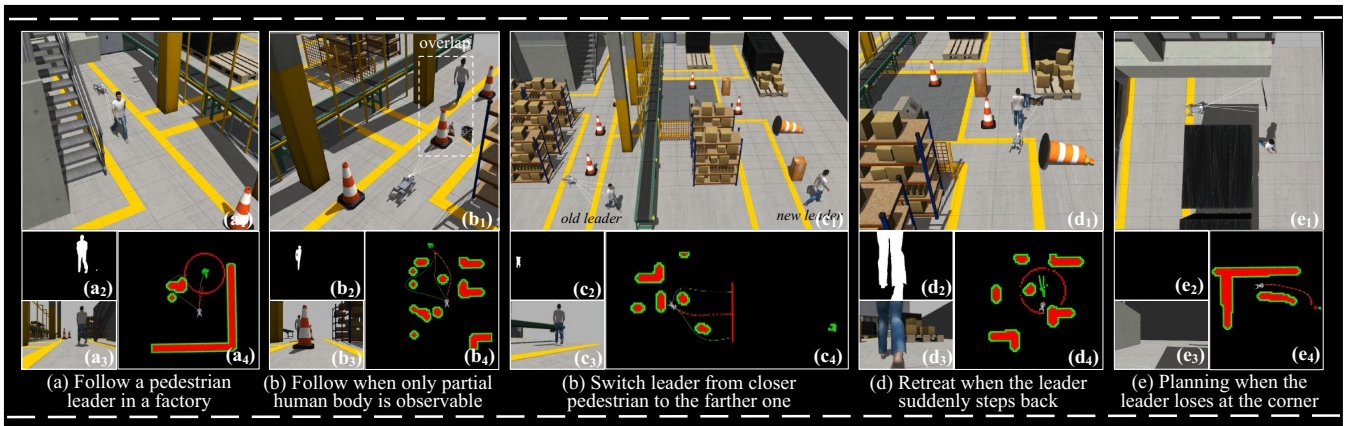


Fig. 6. Simulation for following a pedestrian in a factory. (a–b) The robot follows the leader while navigating around obstacles. (c) Upon receiving a prompt specifying a new leader far away from the robot, the chasing state is activated, and the robot passes underneath the workstation to approach the new leader. (d) When the leader steps backward, the robot also retreats to maintain a safe distance. (e) When the leader turns a corner and leaves the robot’s FOV, the planning state is triggered to search for the leader.

After the UAV detours around two obstacles, as shown in Fig.5(b), the graph-based planner generates multiple feasible trajectories and selects the fastest one, rather than simply replicating the UAV’s historical path. This strategy helps the robot maintain a close distance to the leader. As shown in Table.I and Fig.7, our method achieves the lowest average distance of 2.0 meters and robustly maintains it with the smallest variance, which reduces the likelihood of the leader leaving the robot’s FOV (too close can cause the UAV to leave the robot’s view, too far makes it hard to recognize), thus improving the overall follow success rate.

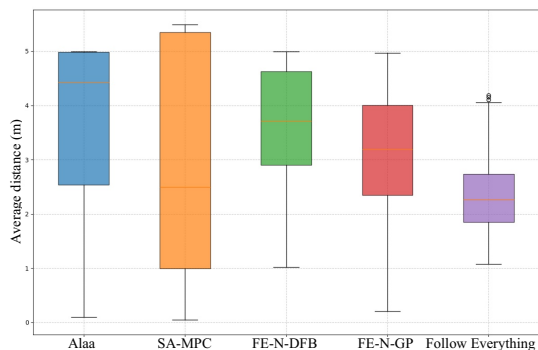


Fig. 7. Average distance between the robot and the leader in 160 tests.

When the gap between obstacles is sufficiently wide for the robot to pass through, as shown in Fig.5(c), the robot directly moves through it in order to maximize efficiency.

Pedestrian leader in factory. In this scenario, the leader is a pedestrian, and the environment contains various obstacles with diverse shapes, sizes, and heights. As shown in Fig.6(a), due to the relatively large size of the leader, it is frequently partially observed by the robot, as shown in (b). This partial observation, combined with frequent visibility loss during obstacle avoidance and the visual similarity between parts of the obstacles and parts of the pedestrian’s body, pose a great challenge for the leader detection/segmentation.

Fig.6(c) demonstrates the performance of the switching state. Upon receiving the prompt "follow the pedestrian on the left", the robot switches its target to a different pedestrian far away from it. Given the large distance between the robot and the new leader, the chasing state is activated. The robot moves at its maximum speed and passes underneath a workstation to rapidly approach the new leader.

Fig.6(d) illustrates the retreating state, where the leader actively steps backward. The robot is expected to retreat accordingly while avoiding nearby construction cones. This behavior significantly enhances safety. As a result, Follow Everything achieves a collision rate of only 1.8%, which is substantially lower than that of other methods. A key perception challenge in this state is that when the leader is close to the robot, only a portion of the leader’s body is visible. The YOLO-based method struggles to recognize such partial views as the leader, resulting in a high collision rate of 80.6%. Moreover, when the leader starts moving forward again, SAM2 without a distance frame buffer often fails to

TABLE I
COMPARISON RESULT

	Follow success rate [↑]	Average leader loss time ratio [↓]	Collision rate [↓]	Average distance [↓]
Alaa (baseline) [13]	21.8%	23.8%	66.9%	3.3 m
SA-MPC (baseline) [21]	11.9%	55.3%	80.6%	2.4 m
FE-N-DFB (ablation)	62.5%	44.0%	25.0%	3.1 m
FE-N-GP (ablation)	81.3%	20.0%	16.3%	2.6 m
Follow Everything (ours)	96.9%	10.7%	1.8%	2.0 m

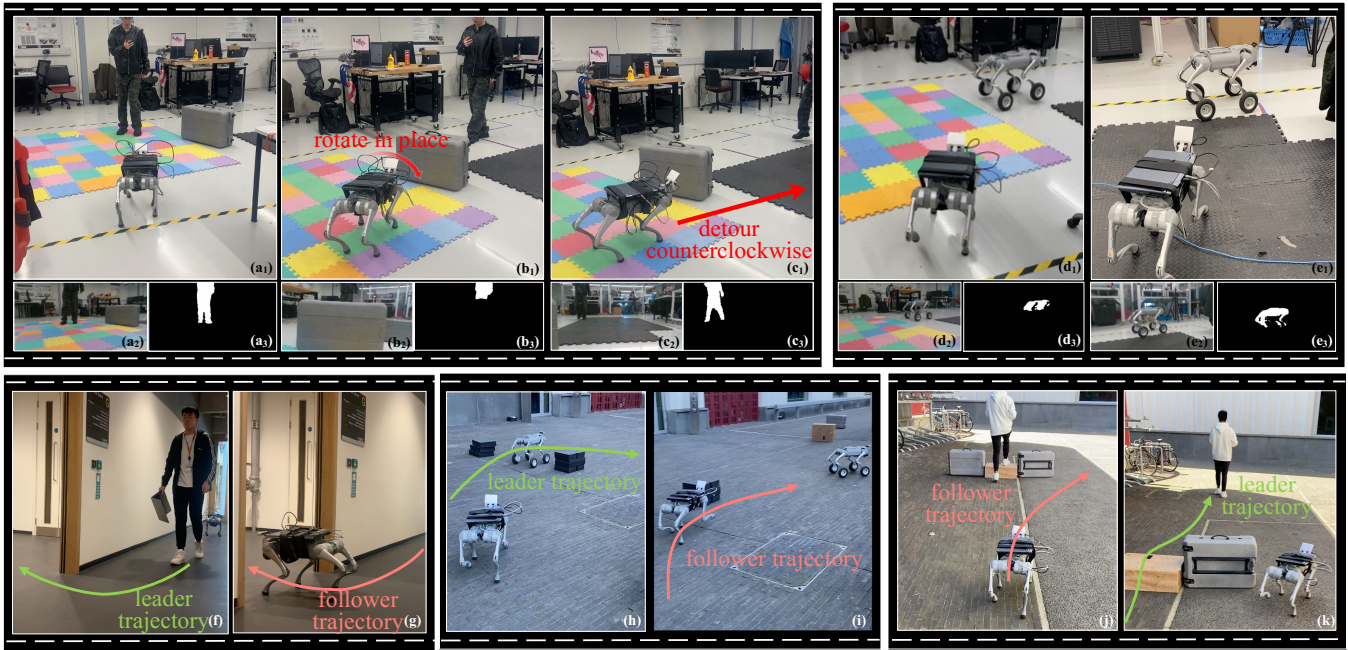


Fig. 8. Illustration of real-world experiments in indoor (a-g) and outdoor (h-k) scenarios. (a-c) While following a pedestrian, maintaining an appropriate safe distance allows the robot to rotate in place and avoid unnecessary detours. (d-e) When following another robot, the leader is reliably identified and followed. (f-g) The planning state allows the robot to follow and re-identify the leader after moving out of the room. (h-i) Instead of replicating the leader’s historical trajectory, the robot takes a shorter path to quickly approach the leader. (j-k) The alternation between following and planning states enables the robot to follow the leader while avoiding obstacles when the leader steps over a box.

re-identify the leader, leading to a collision rate of 66.9% in Alaa. and 25.0% in FE-N-DFB.

Fig.6(e) shows how the planning state contributes to maintaining robust following behavior after the leader turns a corner and temporarily disappears from the robot’s FOV.

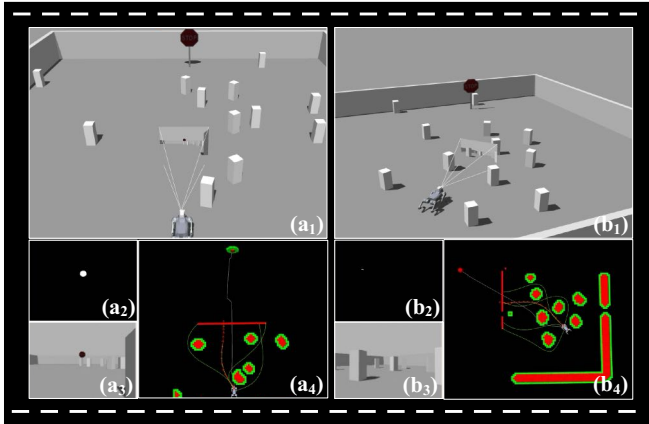


Fig. 9. Simulation for following a stop sign. The graph-based planner provides multiple candidate trajectories so that a safer one can be identified.

Stop sign leader in dynamic scenario. In this scenario, the leader is a stop sign, and dynamic obstacles move randomly, changing their velocities every 3 seconds. The graph-based planner enables the generation of multiple candidate trajectories, ensuring that a safer trajectory is not only available but also selected. This capability allows Follow Everything to significantly outperform other methods, achieving the lowest collision rate of 1.8%.

V. REAL-WORLD EXPERIMENT

In the experiment, the same legged robot is used as the follower, with a person or a wheel-legged robot as the leader. The experiment is conducted in both indoor and outdoor environments. A laptop with Intel i7 and Nvidia RTX 3070 is mounted on the legged robot as the onboard computer.

Following state in indoor scenario. As shown in Fig.8(a), a suitcase obstacle is placed in the center of the scene, and the robot first follows the pedestrian, maintaining a relatively stable safe distance. As shown in Fig.8(b), during the pedestrian’s clockwise detour around the obstacle, the robot continuously stays in the following state, adjusting its orientation to always face the leader while maintaining a safe distance, thus avoiding unnecessary detours. As shown in Fig.8(c), once the pedestrian moves towards a further location, the robot detours counterclockwise around the obstacle and continues to follow the pedestrian. As shown in Fig.8(d-e), when the pedestrian leader is replaced by a legged robot with wheels, the robot’s following behavior remains stable.

Planning state in indoor scenario. As shown in Fig.8(f-g), the robot initially follows the pedestrian’s movement. Once the person exits the room, the planning state is activated, and the robot moves to the last known position of the leader and successfully re-identifies the leader.

Following state in outdoor scenario. As shown in Fig.8(h-i), the leader is a legged robot with wheels, moving between two obstacles and then turning right. By maintaining a safe distance from the leader, the robot avoids replicating the leader’s historical path and instead turns right to quickly approach the leader.

Planning state in outdoor scenario. As shown in Fig.8(j-k), the leader is a pedestrian, moving in front of the robot and then stepping over a box. To avoid collision, the following state enables the robot to turn right and detour around the obstacles. During this process, the pedestrian temporarily leaves the robot's FOV, and the planning state ensures the robot continues detouring until the leader reappears in the robot's FOV, triggering the following state again.

VI. CONCLUSION

This paper presents a unified framework for robust and flexible leader-following. First, in the perception module, a segmentation-based model is employed instead of traditional detection methods, enabling the robot to follow any type or shape of leader. Furthermore, a distance frame buffer is integrated into the segmentation model to address the challenge of retracing the leader after temporary occlusions or short-term loss within the robot's field of view. Second, a goal-aware adaptation is proposed, which dynamically adjusts parameters and generates trajectories appropriate goal states. This allows the robot to adapt its behavior according to the leader's motion state, effectively reducing the risk of losing the leader or causing collisions.

Comprehensive simulations and real-world experiments were conducted using a legged robot as the follower and various objects as the leader—including UAVs, mobile robots, pedestrians, stop signs, and other legged robots—in both indoor and outdoor environments. The results demonstrate that the proposed approach greatly improves the success rate of following, reduces the duration of visual loss of the leader, reduces the collision rate, and decreases the average distance between the robot and the leader. Overall, the framework achieves higher levels of efficiency, safety, and robustness.

REFERENCES

- [1] J. Lee, M. Bjelonic, A. Reske, L. Wellhausen, T. Miki, and M. Hutter, "Learning robust autonomous navigation and locomotion for wheeled-legged robots," *Science Robotics*, vol. 9, no. 89, p. eadi9641, 2024.
- [2] K. Kim, A. Deb, and D. J. Cappelleri, "P-agnav: Range view-based autonomous navigation system for cornfields," *IEEE Robotics and Automation Letters*, vol. 10, no. 4, pp. 3366–3373, 2025.
- [3] L. Roy, E. A. Croft, A. Ramirez, and D. Kulić, "Gpt-driven gestures: Leveraging large language models to generate expressive robot motion for enhanced human-robot interaction," *IEEE Robotics and Automation Letters*, vol. 10, no. 5, pp. 4172–4179, 2025.
- [4] S. Huang, H. Zeng, W. Lan, and X. Yu, "Leader-follower formation tracking control of mobile robots: A visual observer-based approach," *IEEE Transactions on Control Systems Technology*, pp. 1–9, 2025.
- [5] A. Eirale, M. Martini, and M. Chiaberge, "Human following and guidance by autonomous mobile robots: A comprehensive review," *IEEE Access*, vol. 13, pp. 42214–42253, 2025.
- [6] J. Lee, M. Bjelonic, A. Reske, L. Wellhausen, T. Miki, and M. Hutter, "Learning robust autonomous navigation and locomotion for wheeled-legged robots," *Science Robotics*, vol. 9, no. 89, p. eadi9641, 2024.
- [7] J. Terven, D.-M. Córdova-Esparza, and J.-A. Romero-González, "A comprehensive review of yolo architectures in computer vision: From yolov1 to yolov8 and yolo-nas," *Machine learning and knowledge extraction*, vol. 5, no. 4, pp. 1680–1716, 2023.
- [8] T. Yin, X. Zhou, and P. Krahenbuhl, "Center-based 3d object detection and tracking," in *Proceedings of the IEEE/CVF conference on computer vision and pattern recognition*, 2021, pp. 11784–11793.
- [9] X. Wang, C. Fu, Z. Li, Y. Lai, and J. He, "Deepfusionmot: A 3d multi-object tracking framework based on camera-lidar fusion with deep association," *IEEE Robotics and Automation Letters*, vol. 7, no. 3, pp. 8260–8267, 2022.
- [10] Z. Meng, X. Xia, R. Xu, W. Liu, and J. Ma, "Hydro-3d: Hybrid object detection and tracking for cooperative perception using 3d lidar," *IEEE Transactions on Intelligent Vehicles*, vol. 8, no. 8, pp. 4069–4080, 2023.
- [11] Q. Li, R. Li, K. Ji, and W. Dai, "Kalman filter and its application," in *2015 8th International Conference on Intelligent Networks and Intelligent Systems (ICINIS)*, 2015, pp. 74–77.
- [12] Y. Zhang, T. Cheng, R. Hu, L. Liu, H. Liu, L. Ran, X. Chen, W. Liu, and X. Wang, "Evf-sam: Early vision-language fusion for text-prompted segment anything model," *arXiv preprint arXiv:2406.20076*, 2024.
- [13] A. Maalouf, N. Jadhav, K. M. Jatavallabhula, M. Chahine, D. M. Vogt, R. J. Wood, A. Torralba, and D. Rus, "Follow anything: Open-set detection, tracking, and following in real-time," *IEEE Robotics and Automation Letters*, vol. 9, no. 4, pp. 3283–3290, 2024.
- [14] P. T. Singamaneni, P. Bachiller-Burgos, L. J. Manso, A. Garrell, A. Sanfeliu, A. Spalanzani, and R. Alami, "A survey on socially aware robot navigation: Taxonomy and future challenges," *The International Journal of Robotics Research*, vol. 43, no. 10, pp. 1533–1572, 2024.
- [15] P. Trautman and A. Krause, "Unfreezing the robot: Navigation in dense, interacting crowds," in *2010 IEEE/RSJ International Conference on Intelligent Robots and Systems*, 2010, pp. 797–803.
- [16] A. Tripathi, M. A. Khan, A. Pandey, P. Yadav, and A. K. Sharma, "Human following robot using ultrasonic sensor," in *2021 3rd International Conference on Advances in Computing, Communication Control and Networking (ICAC3N)*. IEEE, 2021, pp. 764–770.
- [17] Z. Li, B. Li, Q. Liang, W. Liu, L. Hou, and X. Rong, "A quadruped robot obstacle avoidance and personnel following strategy based on ultra-wideband and three-dimensional laser radar," *International Journal of Advanced Robotic Systems*, vol. 19, no. 4, p. 17298806221114705, 2022.
- [18] V. Reijgwart, C. Cadena, R. Siegwart, and L. Ott, "Efficient volumetric mapping of multi-scale environments using wavelet-based compression," *arXiv preprint arXiv:2306.01279*, 2023.
- [19] C. Scheidemann, L. Werner, V. Reijgwart, A. Cramariuc, J. Chomarat, J.-R. Chiu, R. Siegwart, and M. Hutter, "Obstacle-avoidant leader following with a quadruped robot," *arXiv preprint arXiv:2410.00572*, 2024.
- [20] A. Sridhar, D. Shah, C. Glossop, and S. Levine, "Nomad: Goal masked diffusion policies for navigation and exploration," in *2024 IEEE International Conference on Robotics and Automation (ICRA)*. IEEE, 2024, pp. 63–70.
- [21] Y. Song, Q. Zhang, Z. Hu, and J. Liu, "Safe and robust human following for mobile robots based on self-avoidance mpc in crowded corridor scenarios," in *2023 IEEE International Conference on Robotics and Biomimetics (ROBIO)*, 2023, pp. 1–6.
- [22] Q. Zhang, Z. Hu, Y. Song, J. Pei, and J. Liu, "The human gaze helps robots run bravely and efficiently in crowds," in *2023 IEEE International Conference on Robotics and Automation (ICRA)*, 2023, pp. 7540–7546.
- [23] Z. Zhang, J. Yan, X. Kong, G. Zhai, and Y. Liu, "Efficient motion planning based on kinodynamic model for quadruped robots following persons in confined spaces," *IEEE/ASME Transactions on Mechatronics*, vol. 26, no. 4, pp. 1997–2006, 2021.
- [24] R. Han, S. Wang, S. Wang, Z. Zhang, J. Chen, S. Lin, C. Li, C. Xu, Y. C. Eldar, Q. Hao *et al.*, "Neupan: Direct point robot navigation with end-to-end model-based learning," *IEEE Transactions on Robotics*, 2025.
- [25] Z. Zhu, Q. Zhang, Y. Song, Y. Yang, and J. Liu, "Stc-teb: Spatial-temporally complete trajectory generation based on incremental optimization," *IEEE Robotics and Automation Letters*, 2024.
- [26] Q. Zhang, W. Luo, Z. Zhang, Y. Wang, and J. Liu, "Ga-teb: Goal-adaptive framework for efficient navigation based on goal lines," 2024.
- [27] O. de Groot, L. Ferranti, D. M. Gavrilu, and J. Alonso-Mora, "Topology-driven parallel trajectory optimization in dynamic environments," *IEEE Transactions on Robotics*, vol. 41, pp. 110–126, 2025.
- [28] S. Bhattacharya, "Search-based path planning with homotopy class constraints," in *Proceedings of the AAAI conference on artificial intelligence*, vol. 24, no. 1, 2010, pp. 1230–1237.
- [29] C. Rösmann, F. Hoffmann, and T. Bertram, "Integrated online trajectory planning and optimization in distinctive topologies," *Robotics and Autonomous Systems*, vol. 88, pp. 142–153, 2017.